

Particle and thermohydraulic maldistribution of nanofluids in parallel microchannel systems

Lakshmi Sirisha Maganti¹ · Purbarun Dhar^{1,2} · T. Sundararajan¹ · Sarit K. Das^{1,2}

Received: 30 March 2016 / Accepted: 21 June 2016 / Published online: 12 July 2016
© Springer-Verlag Berlin Heidelberg 2016

Abstract A deep understanding of fluidic maldistribution in microscale multichannel devices is necessary to achieve optimized flow and heat transfer characteristics. A detailed computational study has been performed using an Eulerian–Lagrangian twin-phase model to determine the concentration and thermohydraulic maldistributions of nanofluids in parallel microchannel systems. The study reveals that nanofluids cannot be treated as homogeneous single-phase fluids in such complex flow situations, and effective property models drastically fail to predict the performance parameters. To comprehend the distribution of the particulate phase, a novel concentration maldistribution factor has been proposed. It has been observed that the distribution of particles does not entirely follow the fluid flow pattern, leading to thermal performance that deviates from those predicted by homogeneous models. Particle maldistribution has been conclusively shown to be due to various migration and diffusive phenomena such as Stokesian drag, Brownian motion and thermophoretic drift. The implications of particle distribution on the cooling performance

have been illustrated, and *smart fluid* effects (reduced magnitude of maximum temperature in critical zones) have been observed for nanofluids. A comprehensive mathematical model to predict the enhanced cooling performance in such flow geometries has been proposed. The article clearly highlights the effectiveness of discrete phase approach in modeling nanofluid thermohydraulics and sheds insight on the specialized behavior of nanofluids in complex flow domains.

Keywords Parallel microchannels · Nanofluid · Discrete phase model · Heat transfer · Maldistribution · Brownian · Thermophoresis

1 Introduction

Miniaturization of microelectronic devices and systems coupled with increased functionalities poses severe challenges to cooling technologies due to the generation of high heat fluxes. Conventional cooling techniques prove to be inadequate, and improper thermal management in such cases might lead to device failure. Heat exchange devices, in which a cooling fluid flows through a large number of parallel, micromachined or etched conduits, are commonly employed to cool modern electronic components like MEMS, VLSI circuits, laser diode arrays, high-energy mirrors and other compact products with high thermal loads. Microscale flows ensure higher levels of absorption of energy per unit volume and also provide enhanced values of convective heat transfer coefficient per unit volume. Hence, over the last two decades, microchannel flows have become a major focus of thermofluidics research.

In a pioneering work, Tuckerman and Pease (1981) proposed a novel cooling technique using microchannel heat

✉ T. Sundararajan
tsundar@iitm.ac.in

✉ Sarit K. Das
skdas@iitrpr.ac.in

Lakshmi Sirisha Maganti
lakshmisirisha.maganti@gmail.com

Purbarun Dhar
purbarun@iitrpr.ac.in

¹ Department of Mechanical Engineering, Indian Institute of Technology Madras, Chennai 600036, India

² Present Address: Department of Mechanical Engineering, Indian Institute of Technology Ropar, Rupnagar 140001, India

exchangers which are capable of dissipating large amounts of heat from small areas with high heat transfer rates and less operating fluid requirements. Later, several researchers critically examined the applicability of conventional fluidics theories on microchannel flow domains (Weilin and Mudawar 2002; Qu et al. 2000; Judy et al. 2002). It has been shown that the classical Navier–Stokes equations can be utilized for accurate prediction of liquid flow characteristics in microchannels. Though some discrepancies remain, these have been associated with factors such as measurement inaccuracies, imperfections induced during test section and geometry fabrication, entrance/exit/bend effects and effects of surface roughness. However, despite all such positives, the overall thermal performance of parallel microchannel cooling systems is often reduced because of non-uniform distribution of the working fluid from the manifold to the channels. Thereby, it becomes imperative to properly understand the flow maldistribution behavior in systems that employ microchannel flow cooling, since grossly non-uniform cooling can lead to device failure.

The extent of flow maldistribution in macro- and microchannels is well understood from several proposed models (Bassiouany and Martin 1983a, b; Maharudrayya et al. 2006). However, such models fail to predict maldistribution of flow in parallel microchannels reported by Siva et al. (2014), since they neglect either frictional effects within the channels or the inertial effects in the manifold, while both effects are actually quite important. There are several experimental and numerical reports that attempt to understand flow distribution of single-phase flows in parallel microchannels (Jones et al. 2008; Seghal et al. 2011; Kumaraguruparan et al. 2011), for both adiabatic and heat transfer situations. Based on experiments and computations, Siva et al. (2013) proposed an optimum configuration to reduce single-phase flow maldistribution in parallel microchannel cooling systems.

In recent years, focus has shifted toward obtaining higher thermal transport by modification of the flow field or the fluid itself. Strategies such as enhancement of heat transfer using offset fins or employing nanofluids as working fluids (Bejan and Morega 1993; Singh et al. 2011) have been practically implemented. Nanofluids, which are engineered colloidal suspensions of metallic and/or ceramic nanoparticles in a conventional base fluid, exhibit thermal conductivity values which are 20–150 % higher than those of the base fluids reported by Choi and Eastman (1995). Several experimental and theoretical works have been reported on the enhanced thermal conductivity of nanofluids (Dhar et al. 2013a, b; Lee et al. 1999; Koo and Kleinstreuer 2004) over the past decade. The thermal transport caliber of any nanofluid depends mainly on nanoparticle concentration, thermal conductivity, diameter of particles, base fluid conductivity and temperature Das et al. (2003).

Several studies (Das et al. 2006; Özerinç et al. 2010) have conclusively reported that nanofluids show great promise for use in cooling technologies.

The use of nanofluids in microchannel heat exchangers has been recommended as a potentially feasible solution for cooling microelectronic devices. There are several experimental and numerical investigations that highlight the enhanced heat transfer characteristics and pressure drop of nanofluids in parallel microchannel systems (Chen and Ding 2011; Kalteh et al. 2011; Hung et al. 2012; Raisi et al. 2011). It has been reported that enhanced heat transfer can be achieved with the use of nanofluids in microchannels but at the cost of increased pressure drop. Further, the mechanisms involved in the heat transport phenomena are not fully understood, requiring more analysis (Salman et al. 2013; Mohammed et al. 2011). There are few reports which concentrate on the modeling of flow and heat transfer characteristics of nanofluids in microchannels, but all these consider nanofluids as homogeneous single-component fluids for analysis; this has been conclusively reported by Singh et al. (2011) to be an inefficient and incorrect assumption. Unlike macro-size particles, the nanoparticles migrate under the influence of a variety of factors such as temperature, temperature gradient, shear gradient and pressure gradient. Therefore, the concentration of the nanoparticle phase varies in a non-trivial manner, often not in line with the flow pattern. The resulting heat transfer characteristics of nanofluids are also complex, particularly for non-simple flow patterns.

A detailed survey of literature reveals that there are no studies which highlight the effects of flow and particle concentration distributions of nanofluids (treated as non-homogeneous multicomponent fluids) in parallel microchannels. So there is a need to carry out an in-depth study to understand the effects of nanofluid maldistribution along with non-uniform nanoparticle concentration and temperature in parallel microchannel cooling systems. Such a study is expected to directly contribute toward the design and optimization of microchannel systems which employ nanofluids for cooling.

2 Numerical formulation

A detailed numerical investigation of the flow and heat transfer in alumina–water nanofluid in a parallel microchannel system has been carried out, to understand the associated concentration and thermohydraulic maldistributions. There are two different approaches used in the present work, namely the effective property modeling (EPM) and the discrete phase modeling (DPM) or Eulerian–Lagrangian approach. The former one considers the nanofluid as a single-phase homogeneous fluid with effective

physical properties which are linear functions of fluid and particle material properties. The latter considers nanofluid as a two-phase non-homogeneous fluid, i.e., dispersed nanoparticle phase transported by the continuous fluid phase. This formulation considers all the prevalent diffusion and migration mechanisms of the nanoparticles within the fluid, such as hydrodynamic forces, Brownian and thermophoretic diffusion and shear-induced migration. The work also critically examines the need for the computationally intensive DPM approach to model the nanofluid behavior in microchannel systems.

2.1 Governing equations for the continuous phase

The governing equations for the EPM and the continuous phase of the DPM are the continuity equation (mass), Navier–Stokes equation (momentum) and energy equation, which are summarized below.

$$\frac{\partial \rho}{\partial t} + \nabla \cdot (\rho \vec{V}) = 0 \tag{1}$$

$$\frac{\partial \rho \vec{V}}{\partial t} + \nabla \cdot (\rho \vec{V} \vec{V}) = -\nabla P + \nabla \cdot (\mu (\nabla \vec{V} + \nabla V^T)) + S_m \tag{2}$$

$$\rho C \left[\frac{\partial T}{\partial t} + \vec{V} \cdot \nabla T \right] = \nabla \cdot [k \nabla T] + S_e \tag{3}$$

In Eqs. (1)–(3), t represents time, g is the acceleration due to gravity, p is the pressure, T is the temperature, and V is the velocity of the fluid. Also ρ , C and k represent the density, specific heat and thermal conductivity of the continuous phase fluid. The effects of viscous dissipation and work due to compressibility are assumed to be negligible in the energy equation. The source terms, S_m and S_e , represent the momentum and energy exchanges, respectively, between the continuous phase (fluid) and the discrete phase (nanoparticles). These terms are zero for the homogeneous single-phase model (i.e., EPM).

2.2 Governing equations for the dispersed phase

The particle trajectories in the flow field are determined by the Newton’s second law of motion. Considering a Lagrangian frame of reference, the governing equation (in Cartesian coordinates) for the motion of the nanoparticles is expressed as:

$$\frac{du_p}{dt} = F_D(u - u_p) + \frac{g(\rho_p - \rho)}{\rho_p} + F \tag{4}$$

where the force per unit mass is given as

$$F = F_B + F_T + F_L + F_P + F_V \tag{5}$$

In the above equation, u_p , u are the particle velocity and fluid phase velocity, respectively. ρ_p , ρ are the nanoparticles density and fluid phase density, respectively. F is the net specific force acting on the particle. The terms F_B , F_T , F_L , F_P and F_V represent the forces due to Brownian motion, thermophoretic drift, Saffman lift, contribution due to pressure gradient and contribution due to virtual mass FLUENT User Manual (2016), respectively. The velocity coefficient (F_D) of drag force exerted by the continuous phase on the particle is evaluated as:

$$F_D = \frac{18 \mu C_D Re}{\rho_p d_p^2} \frac{1}{24} \tag{6}$$

where μ is the fluid viscosity.

For submicron particles of size d_p (as is the present case), the classical form of Stokesian drag needs to be modified so as to accommodate the non-continuum or slip boundary effects particularly for high Knudsen number situations such as the flow past nanoscale particles, at the particle–fluid interface. The modified coefficient for Stokes drag can be expressed as: Ounis et al. (1991)

$$F_D = \frac{18 \mu}{\rho_p d_p^2 C_c} \tag{7}$$

where C_c represents the Cunningham correction factor to Stokes law, given by the expression

$$C_c = 1 + \frac{2\lambda}{d_p} \left(1.257 + 0.4e^{-(1.1d_p/2\lambda)} \right) \tag{8}$$

with λ representing the molecular mean free path.

Since Brownian motion is random in nature with zero net directional flux, a probability function is required to model the force. The amplitude of a Brownian force component is expressed as:

$$F_{B_i} = \zeta_i \sqrt{\frac{\pi S_0}{\Delta t}} \tag{9}$$

where ζ_i is a random number which is part of a Gaussian distribution with zero mean. The amplitudes of the Brownian force components are estimated at each step of the discrete phase calculations. The components of the Brownian randomness are modeled as Gaussian white noise process with the expression for the spectral intensity $S_{n,ij}$ given as Li and Ahmadi (1992)

$$S_{n,ij} = S_0 \delta_{ij} \tag{10}$$

where δ_{ij} is the Kronecker delta function and the amplitude of the spectrum S_0 is expressed as

$$S_0 = \frac{216 \nu k_B T}{\pi^2 \rho d_p^5 \left(\frac{\rho_p}{\rho} \right)^2 C_c} \tag{11}$$

Because of the random nature of the Brownian force, this will result in an additional isotropic diffusion of the nanoparticles within the fluid medium.

The dispersed particles subjected to a temperature gradient in the fluid experience a force in the direction opposite to that of the gradient. This is due to higher degree of molecular bombardment on the particles in the heated region, driving them toward the colder region where the net force from bombardment is less. This phenomenon is known as thermophoresis or Soret effect, and the expression for the force generated due to the thermophoresis drift is expressed as

$$F_T = -D_{T,P} \frac{1}{m_p T} \frac{\partial T}{\partial x} \quad (12)$$

where m_p , T are particle mass and local fluid temperature, respectively.

$D_{T,P}$ is the thermophoretic coefficient Talbot et al. (1980) evaluated through the expression

$$D_{T,P} = \frac{6\pi d_p \mu^2 C_s (k + C_t k_n)}{\rho(1 + 3C_m k_n)(1 + 2k + 2C_t k_n)} \quad (13)$$

The constants, $C_m = 1.146$, $C_s = 1.147$ and $C_t = 2.18$, are the momentum exchange, thermal slip and temperature jump coefficients, respectively. K_n is the Knudsen number and K is the ratio of fluid thermal conductivity to particle thermal conductivity.

The Saffman lift force is generated due to shear on the particle by the continuous phase. This form of lift arises only for small particles in a flow and it is expressed as Saffman (1965)

$$F_L = \frac{2k_s v^{\frac{1}{2}} \rho d_{ij}}{\rho_p d_p (d_{lk} d_{kl})^{1/4}} (u - u_p) \quad (14)$$

where $k_s = 2.594$ is a constant and d_{ij} is the deformation tensor for the continuous phase which governs the net shear force generated on the particle.

The force arising on the particles due to pressure gradient within the fluid is expressed as

$$F_P = \left(\frac{\rho}{\rho_p} \right) u_p \frac{\partial u}{\partial x} \quad (15)$$

The inertia required to propel the fluid surrounding the particles gives rise to a virtual mass force of the form

$$F_V = \frac{1}{2} \frac{\rho}{\rho_p} \frac{d}{dt} (u - u_p) \quad (16)$$

2.3 Effective property model

The following equations have been used for determining the effective properties like density, specific heat, viscosity

and thermal conductivity, respectively, for alumina–water nanofluid Anoop et al. (2009) through the expressions:

$$\rho_{nf} = (1 - \phi)\rho_{bf} + \phi\rho_p \quad (17)$$

$$(\rho C_p)_{nf} = (1 - \phi)(\rho C_p)_{bf} + \phi(\rho C_p)_p \quad (18)$$

$$\mu_{nf} = \mu_{bf}(1 + 10\phi) \quad (29)$$

$$k_{eff} = k_f \frac{[k_p + (n - 1)k_{BF} - (n - 1)\phi(k_{BF} - k_p)]}{[k_p + (n - 1)k_{BF} + \phi(k_{BF} - k_p)]} \quad (20)$$

In the above equations, ϕ is the volume fraction of the nanoparticle phase. With these effective properties, the nanofluid can be approximated by a homogeneous single-component system, in the EPM approach.

2.4 Computational details

A three-dimensional U-type parallel microchannel domain has been created for simulating the fluid flow and heat transfer associated with a nanofluid. The governing equations described for the DPM and EPM approaches have been solved using ANSYS Fluent 14.5. Figure 1a shows the geometrical configuration utilized in the present study. This particular geometry has been shown to have the worst flow distribution characteristics (Siva et al. 2014). Hence, studies conducted with this geometry can provide information on nanofluid flow maldistribution in microchannels for the worst-case scenario. The details of geometry and working fluid are as follows: Hydraulic diameter (D_h) of channel is 100 μm , area ratio ($A_{\text{channel}}/A_{\text{manifold}}$) is 0.2, number of channels (N) is 7, aspect ratio of channel (H/W) is 0.1, working fluid is either water or Al_2O_3 –water nanofluid. A mesh consisting of quadrilateral elements has been utilized. Nanoparticles are injected at the inlet manifold in a spatially and temporally uniform manner, and the maldistributions that develop in the flow within the microchannel ducts are captured. A grid independence study is carried out by considering different number of grid cells. Figure 1b depicts the variation of flow maldistribution parameter (see, Eq. 21) which is considered for the grid independence test. As evident from the figure, there is no change in maldistribution parameter with respect to the number of mesh elements beyond 1,250,000. A finer grid with (with 1,455,237 grid cells) is considered for the present study since availability of large number of surfaces at the inlet to inject more particle streams renders particle tracking more accurate. Uniform heat flux boundary condition has been applied at the bottom and side walls for heat transfer cases, and the top wall has been considered as adiabatic.

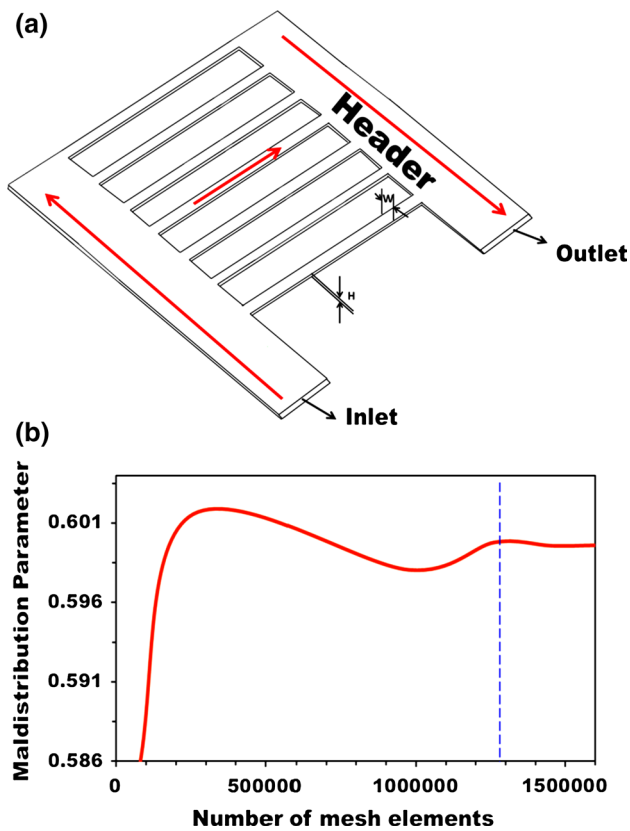


Fig. 1 **a** Geometry of parallel microchannel system used as the simulation domain, **b** grid independence test (maldistribution parameter variation with respect to number of mesh elements)

The present numerical model has been validated with respect to the published results of Siva et al. (2014) and Singh et al. (2011). The former study discusses in detail the flow maldistribution of water in a parallel microchannel system, whereas the latter study provides a comprehensive report on the thermohydraulic performance of nanofluids in a single microchannel system. In the limiting cases of number of channels becoming unity or the inlet nanoparticle concentration becoming zero, the results of the present study are expected to match with those of the earlier studies mentioned above. It is therefore justifiable to validate the nanofluid flow and thermal behavior predicted by the present approach with the results of these two sources mentioned. The corresponding comparison plots have been illustrated in Fig. 2a–c. Figure 2a compares the present microchannel model predictions against the published data of Siva et al. (2014) for the maldistribution of water flow rate among the parallel channels for two different hydraulic diameters (88 and 176 μm) at $Re = 70$. It is observed from Fig. 2a that the present simulations accurately depict the flow maldistribution behavior in parallel microchannel systems. Figure 2b, c illustrates the efficacy of the present model in simulating flow and thermal transport behavior,

in comparison with the available data for nanofluid flow within a single microchannel Singh et al. (2011). It is evident that the present discrete phase model (DPM) agrees well with reported experimental data of Singh et al. (2011). Thus, the present DPM approach has been validated with documented experimental data for the flow of simple fluids and nanofluids in both single as well as multiple microchannel assemblies.

3 Results and discussion

3.1 Adiabatic flows

3.1.1 Pressure drop and flow maldistribution

In case of single-phase fluids, the major challenge to be addressed is often the hydraulic maldistribution in the channel system; however, in the case of non-homogeneous media such as nanofluids, maldistribution of the effective concentration is also expected to pose additional concerns toward the system performance characteristics. Thus, a detailed Eulerian–Lagrangian particle-tracking model is necessary to simulate such flows and to establish the deviations from the predictions of homogeneous property models. Furthermore, it is pertinent that the flow regimes be identified for the system geometry under consideration over which maldistribution effects are appreciably high. Accordingly, the effects of Reynolds number and concentration on flow and particle maldistributions of nanofluids in parallel microchannel systems have been numerically investigated in the present study using the DPM approach. The flow maldistribution can be quantified based on the flow maldistribution factor (FMF) defined as Siva et al. (2014):

$$\eta = \left(1 - \frac{\Delta P_{\min}}{\Delta P_{\max}} \right) \tag{21}$$

where ΔP_{\min} and ΔP_{\max} are the channel-wise minimum and maximum pressure drops.

Similarly, the extent of concentration maldistribution is quantified using the concentration maldistribution factor (CMF) defined as

$$\varepsilon = \left(1 - \frac{\phi_{\min}}{\phi_{\max}} \right) \tag{22}$$

The magnitudes of the FMF and CMF vary between 0 and 1, where 1 represents a scenario of maximal maldistribution (when some channels have no coolant flow or some regions of the flow field are totally devoid of particles).

The present study utilizes a generalized nanofluid formulation throughout. Owing to their excellent transport characteristics and stability, nanofluids based on aluminum oxide particles (40–50 nm) and water have been used Das

Fig. 2 Comparison of present numerical model with reported experimental data **a** validation with experimental results of Siva et al., **b** validation with the experimental results of Singh et al. for adiabatic case, **c** validation with the experimental results of Singh et al. for diabatic case

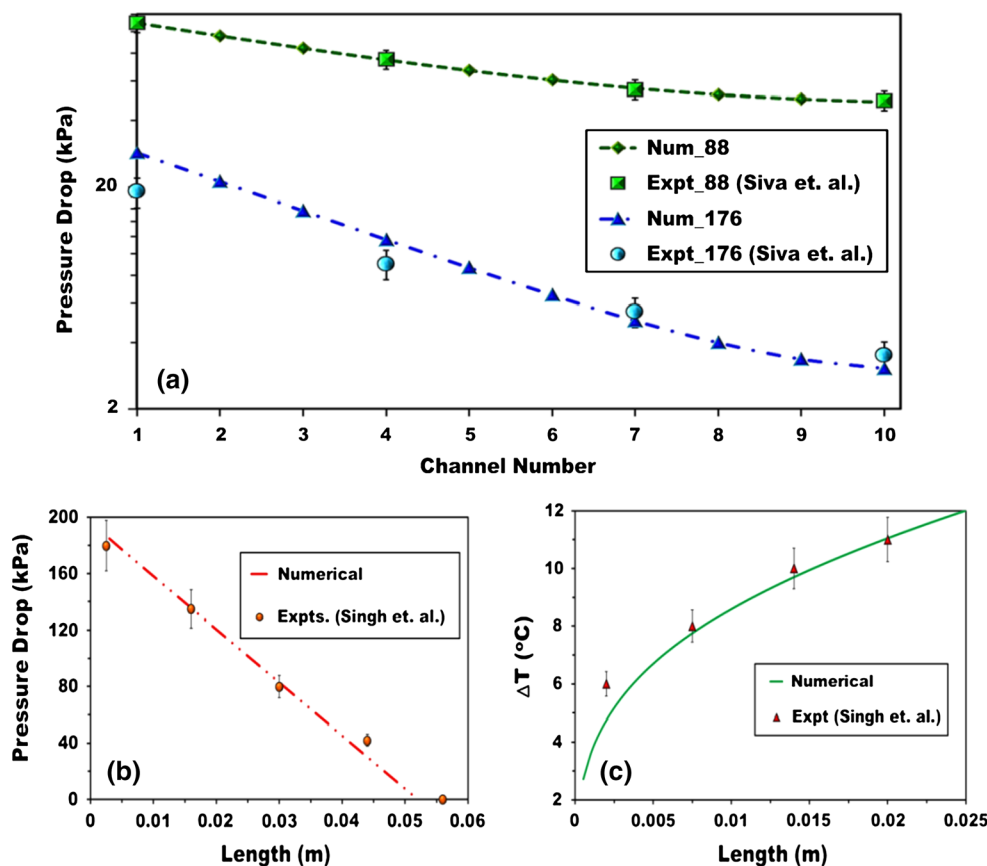


Table 1 Comparison of pressure drop (in Pa) across each channel for three different concentrations (1, 3 and 5 vol%) for water nanofluid

Channel number	$Re = 2$				$Re = 50$			
	Water	1 vol%	3 vol%	5 vol%	Water	1 vol%	3 vol%	5 vol%
1	1871.262	2007.619	2310.916	2531.31	46,785.9	49,849.2	56,953.2	62,196.2
2	1501.764	1607.53	1844.36	2014.9	37,569.3	40,046.5	45,673.6	49,939.4
3	1223.03	1304.63	1491.47	1620.18	30,608.2	32,622.3	37,209.9	40,690.5
4	1017.86	1079.9	1224.31	1333.64	25,480.3	27,109	30,816.2	33,712
5	873.99	919.4	1043.65	1127.62	21,882.7	23,132.1	26,056	28,420.1
6	782.7	817.34	914.87	985.9	19,599.2	20,533.3	22,985.1	25,101.2
7	733.15	757.96	845.8	900.84	18,359.2	19,030.4	21,170.6	23,176.6

et al. (2006). Furthermore, a basic U-type manifold and channel geometry are considered as it has been reported to exhibit the highest maldistribution (compared to I and Z type configurations, Siva et al. 2014) in order to get a clear picture of nanofluid performance in the worst-case scenario. Channel-wise pressure drop, a parameter important to characterize the flow features and pumping requirements in parallel channel systems, has been illustrated in Table 1, for nanofluid medium at three different concentrations (1, 3 and 5 vol%) and for two different Reynolds numbers (2 and 50). As evident from the figure, the pressure drops across the channel are higher for the nanofluid as compared to those of water, because of higher fluid viscosity.

The pressure drop values in the initial channels are higher for both water and nanofluid as compared to those of the end channels. This variation in channel-wise pressure drop is attributed to the non-uniform distribution of flow rate across the different channels (i.e., flow maldistribution). However, knowledge of the pressure drop values in the channels individually does not portray a complete picture regarding the maldistribution characteristics for the overall geometry.

The extent of maldistribution for water and nanofluids has been illustrated in Fig. 3 by the maldistribution parameter (η) at different Reynolds numbers and for different concentrations.

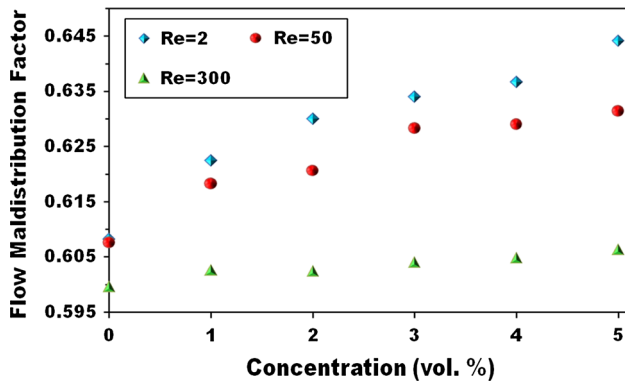


Fig. 3 Variation of FMF (flow maldistribution factor) (η) with respect to concentration at different Reynolds number values

It is observed from the figure that hydraulic maldistribution increases gradually as a function of nanofluid concentration and the effect is further enhanced at lower Reynolds numbers. However, in reality, higher viscosity is expected to give rise to a more uniform distribution; greater flow maldistribution at higher concentration thus provides a strong hint that the behavior of nanofluids is complex. The flow characteristics of nanofluids at low Reynolds numbers seem to be governed by the non-homogeneous distribution of particles caused by various particle migration mechanisms addressed in Eq. 5. At high Reynolds numbers, the flow is dominated by inertia, but the end channels receive a greater share of the working fluid flow. In other words, maldistribution is reduced at high Re because the shear and diffusion-induced migration of nanoparticles are arrested and the particles are forced to follow the streamlines due to higher inertial forces exerted by the fluid flow. Accordingly, the flow maldistribution factor (FMF) becomes independent of nanofluid concentrations at high flow velocities. However, at low Reynolds numbers, the inertia of flow is less, and hence, the random migration of particles due to Brownian motion and shear-induced migration become dominant. Such random motion of nanoparticles leads to increased maldistributions of flow and particle concentrations. For the same reason, flow maldistribution exhibits sensitivity to the particle concentration and the deviation from the base flow increases with increasing particle concentrations at low Reynolds numbers. Another important inference from the above result is that in practical microchannel flows operating in the low Re regime, nanofluids may not behave as homogeneous fluids. Hence, their transport capabilities in microchannel systems cannot be predicted by conventional numerical methods employing effective property models (EPM) wherein the nanofluid is treated as a homogeneous, single-component fluid.

Further insight into the behavior of nanofluids in such complex flow paths can be acquired from the comparison

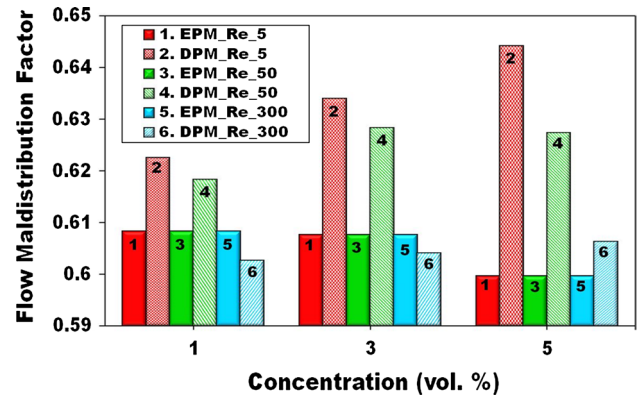
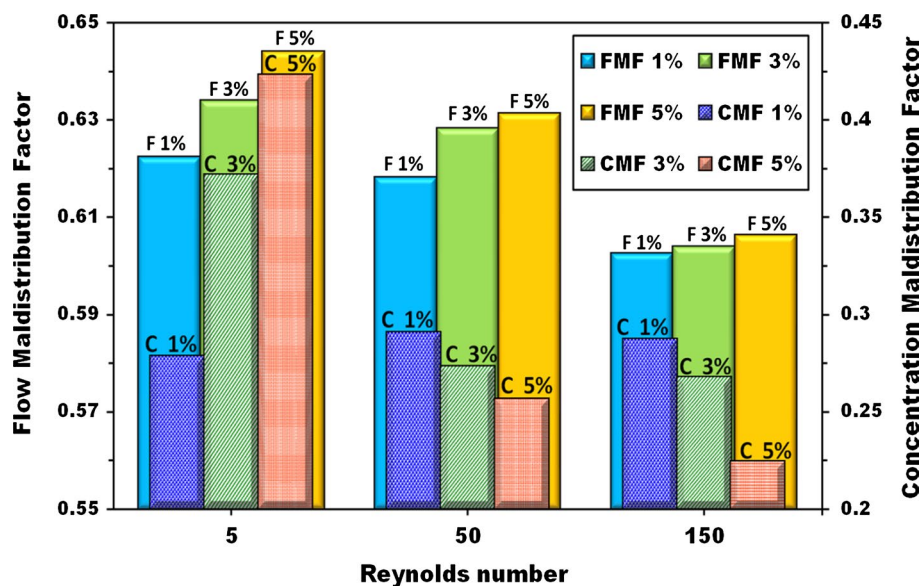


Fig. 4 Comparison of FMF (flow maldistribution distribution) of nanofluid obtained through DPM (discrete phase modeling) and EPM (effective property modeling) approaches at three different concentrations and for three different Re

of maldistribution patterns obtained from DPM and EPM analyses, as illustrated in Fig. 4. The FMF predicted by the EPM remains independent of changes introduced in either the concentration or Re , except for highly concentrated fluids. This anomaly arises due to the EPM's treatment of nanofluid as a homogeneous and single-component fluid medium, wherein fluid properties are calculated based on the effective material properties. From Fig. 4, it is observed that the flow maldistributions predicted at 1 and 3 vol% by the EPM are similar in magnitude and this occurs due to the usage of expressions such as Einstein's or Batchelor's equations Dhar et al. (2013a, b) for determining the viscosity of suspensions in the EPM. These expressions work well only for very dilute suspensions, and the predictions are weakly dependent on concentration, which leads to similar viscosity values in the two cases, leading to similar FMF. However, at 5 %, the viscosity value predicted by the EPM increases marginally, leading to marginal drop in the FMF, but all the predictions remain independent of Re since the distribution of the single-phase nanofluid is unaffected by inertial effects in the range considered. On the contrary, the variation of FMF can be clearly observed to be functions of Re and concentration when DPM is resorted to. These observations are credible as the Eulerian–Lagrangian approach of modeling nanofluids has been reported to predict experimental observations more accurately unlike its single-phase homogeneous fluid approach.

The DPM approach is able to capture the actual variation of FMF since it offers a separate treatment for particle motion and tracks the migration of the particles (considering all the diffusive effects such as Brownian fluctuations, Saffman lift and thermophoresis) within the continuous phase. It is observed in Fig. 4 that increment in concentration at a particular Re leads to increased FMF value for DPM, as opposed to the decreasing trend for EPM.

Fig. 5 Comparison of FMF (flow maldistribution factor) and CMF (concentration maldistribution factor) for the nanofluid at three different Re and concentrations



Enhanced particle population increases the viscosity of the nanofluid, which, in accordance with EPM approach, leads to reduced FMF. However, in the DPM approach, increased particle count per unit volume introduces higher degree of Brownian fluctuations and more drag as well. Exemplary scenario for particle maldistribution can be provided at this instance. If flow in the first channel is considered, the fluid component of the nanofluid gets distributed similar to that of pure base fluid flow. However, owing to higher inertia of the particles (due to the higher density), only a fraction smaller than the average particle concentration enters the first channel. This effectively enhances the concentration of the fluid heading to the next channel. The selective admission of the fluidic phase results in a higher degree of particle maldistribution of flow and particle concentration within the channels. With increasing concentration, this effect becomes more significant, leading to further worsening of flow distribution. Increase in flow Re leads to decreased FMF, and this is caused by the dominance of flow inertia. At higher flow velocities, the diffusive and migration effects of particles lose significance and the particles more or less follow the flow pattern, leading to more uniform distribution. In fact, the DPM predictions for FMF approach those of EPM as Re increases, providing evidence that the nanofluid behavior asymptotically approaches homogeneous fluid behavior in high inertia regimes of the fluid.

3.1.2 Concentration maldistribution

As discussed in the preceding section, it is also important to understand the particle concentration distribution during nanofluid flow in parallel microchannels, since it directly affects the cooling performance. Common intuition,

considering nanofluids to be similar to single-phase systems, suggests that the nanofluid should distribute similar to the base fluid; however, this assumption is not supported by the DPM predictions. Figure 5 illustrates a comparison between the FMF and concentration maldistribution factor (CMF) for different concentrations and Re . It can be inferred from the figure that nanofluids do not behave like homogeneous fluids as the FMF and CMFs are grossly dissimilar at different Re and inlet concentrations. While the trends of both flow and concentration maldistributions are qualitatively similar at low Re , they are absolutely different at high Re . In fact, Fig. 5 provides further evidence for the failure of the EPM and the process by which the maldistribution of concentration, in turn, leads to a non-intuitive pattern of flow maldistribution. While the FMF is expected to reduce for concentrated nanofluids owing to higher viscosity, the reverse trend is observed.

At low Re , the particles are more independent to migrate and randomly diffuse across the streamlines; this in turn leads to non-uniform distribution of concentration. As the particle loading increases, the migration effects, fluidic drag and inter-particle interactions increase, thereby causing higher CMF. As a consequence, the flow maldistribution also increases, as discussed in the preceding section. At high Reynolds numbers, EPM predicts no noticeable changes in the FMF from that of low Re ; however, DPM predicts appreciable changes. While the decrease in FMF compared to low Re scenario can be justified based on the higher inertia of flow which reduces particle migration effects, the decrease of CMF at higher Re with increasing concentrations calls for a deeper insight. Increase of Re at a fixed hydraulic diameter causes the flux of the fluid to increase, and accordingly, the streamlines are packed closer. In such cases, although inertia reduces diffusive

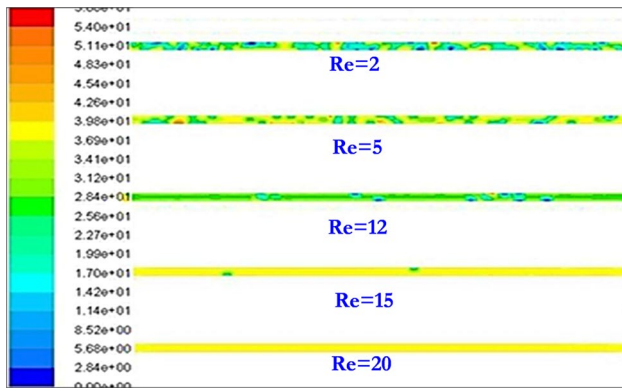


Fig. 6 Contours of concentration distribution at inlet cross section of inlet manifold. At different Re ($Re = 2, 5, 12, 15$ and 20) for 1 vol% with Brownian diffusion active within the DPM (discrete phase modeling) formulation

particle movements orthogonal to the streamlines severely, the particles still have scope to diffuse and migrate along the direction of flow. This effect still leads to uneven distribution, and hence at low particle populations, the CMF remains fairly unaffected. However, as the concentration is increased, the particle population is dense within the closely placed streamlines and migratory particle movements along the streamlines are also restricted due to excessive particle loadings in the system. The system thus begins to behave like a bed of granular media and particle motion more or less follows that of the base fluid, thereby reducing the concentration maldistribution. This effect is further pronounced at higher Re values, and the CMF at high concentration further decreases.

A qualitative assessment of the impact of the particle slip forces on the concentration maldistribution can be made from the maldistribution pattern at the entrance section of the inlet manifold. The concentration distribution contours at different Re have been shown in Fig. 6. A non-uniform concentration distribution can be observed to prevail at the entrance of the inlet manifold at low Re , and the uniformity of concentration distribution improves as Re increases. The diffusion or migration of particles in the region near the entrance of the manifold is primarily due to Brownian motion, since in this region, it is the only slip mechanism which is existent (at the inlet, flow is yet to be established, and hence, drag, lift is of less importance). At very low Re , the inertia of the continuous phase is small in magnitude and the Brownian velocity of particles is comparable with the continuous phase velocity. Hence, diffusion or migration of the particles away from the streamlines takes place spontaneously, leading to non-uniform distribution of concentration at the entrance of the manifold itself. This effect diminishes as the Re increases and the phenomenon is

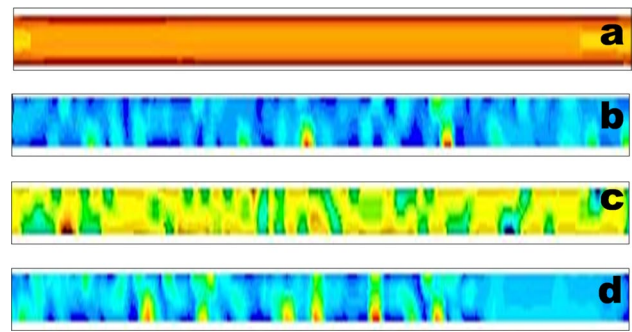


Fig. 7 Particle concentration variation across the inlet and exit sections, **a** entrance of the inlet manifold with Brownian effect switched off at $Re = 2$, **b** exit of the outlet manifold with Brownian effect switched off, **c** entrance of the inlet manifold with Brownian effect incorporated, **d** exit of the outlet manifold with Brownian effect incorporated

observed only when the ratio of continuous phase velocity (V_C) to Brownian velocity (V_B) is below 500 ($V_C/V_B < 500$).

To justify the above observations, simulations have also been carried out by switching off the Brownian component in the governing equations and Fig. 7 illustrates the corresponding results. Figure 7a, b exhibits the concentration distribution contours at the entrance and exit of the inlet and outlet manifolds, respectively, without the Brownian effect. Figure 7c, d illustrates the same with the Brownian effect incorporated. While the outlets show some similarities in the distribution pattern, the inlets are grossly dissimilar and the effect of Brownian motion on particle maldistribution can be clearly understood. Brownian motion is evidently one of the most important phenomena in low Re flows of nanofluids in microscale flow devices.

The effect of flow inertia on the distribution of the nanofluid and its implications vis-à-vis concentration maldistribution among the individual channels can be understood from the concentration contours plotted for specific channel inlets at different Re values. Figure 8 illustrates the cross-sectional concentration contours at regions very near the inlets of channels 3, 5 and 7 for three different Re . At low Re , the inertia of the fluid within the inlet manifold is low, thereby allowing the front channels to get a high share of the particle population than the case at higher Re , where majority of the particle population is flushed to the later channels. This can be observed in Fig. 8, where the concentration contour in channel 3 at higher Re is much more diffused and has no particle aggregations as seen in low Re situations. Channel 5, falling within the central region, experiences very little change in distribution pattern with changing Re value. At low Re , a large extent of the particles enter into the front channels, and at high Re , they travel toward the end channels, providing the central

Fig. 8 Effect of flow inertia on the concentration distribution within individual channels (at a section proximal to the channel inlet) for nanofluid of a fixed concentration

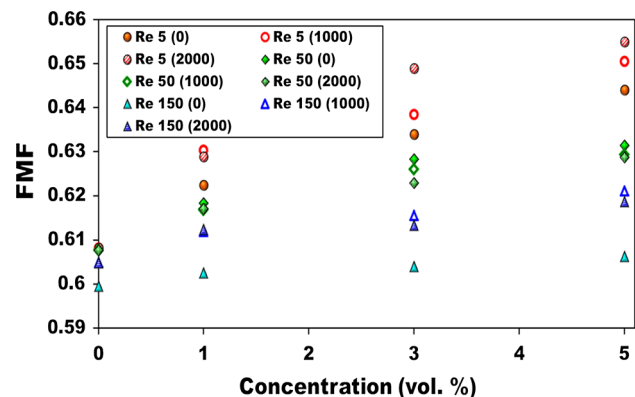
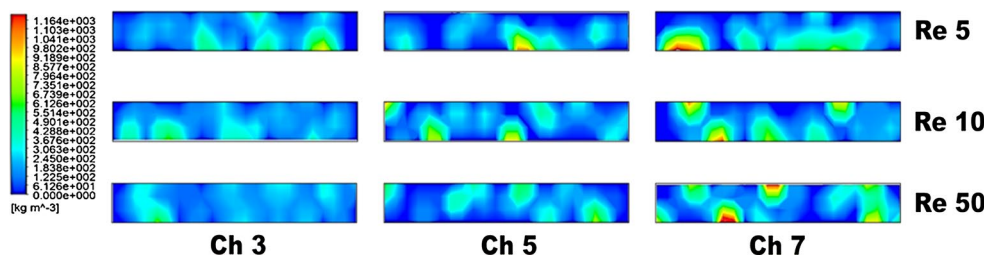


Fig. 9 FMF (flow maldistribution factor) variation for nanofluids with respect to concentration at three different heat fluxes and three Re values

channels with essentially the same share of particles. At low Re , the last channel gets a dilute flow, as observed in the figure, where significant fractions of particle free zones can be observed. As the Re increases, convective flushing pushes more particles to the end channels, and as evident from the figure, the distribution in channel 7 at moderate and high Re improves drastically compared to that in the low inertia regime. In the context of cooling technologies, probability of occurrence of hot spots can be deduced to be low among the regions housing the central channels for all flow regimes.

3.2 Diabatic flows

3.2.1 Flow maldistribution

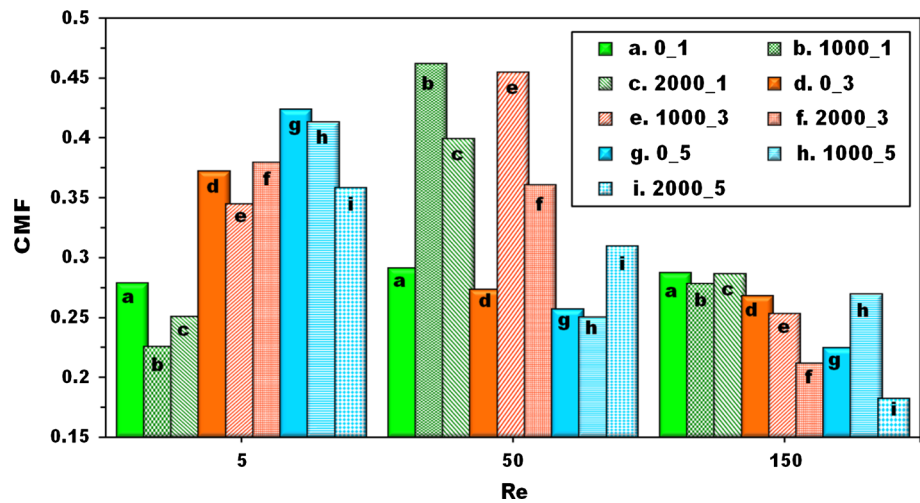
Although understanding flow maldistribution is important for optimizing the pumping characteristics, understanding the same with increasing heat loads is required for efficient design of such specialized microscale flow systems. Figure 9 illustrates the FMF variation for nanofluids as a function of concentration, Re and imposed heat flux. As already pointed out for the adiabatic cases, the presence of nanoparticles in the base fluid changes the trend of fluid distribution among the parallel microchannels and the effect is more pronounced at low Re . Furthermore, the deterioration of FMF at a particular Re with increasing

temperature is more in the case of nanofluid than that of water, which brings to the forefront the important role of nanoparticle migration and diffusion (which are more prominent at elevated temperatures) in determining the overall flow pattern. As heat flux increases, the temperature in the system increases, giving rise to a more non-uniform distribution of fluid because of the increased role played by particle migration over fluid convection. However, the increment of FMF for water with respect to Re and heat flux is negligibly small. On the contrary, the FMF increases appreciably for the nanofluids (DPM simulation) with Re , heat flux and concentration; the increase in FMF is more at low Re with respect to both heat flux and concentration. At low Re , as discussed earlier, resistance to the random motion of particles due to Brownian fluctuations is less and the Brownian velocity of the particles is comparable to the continuous phase velocity. This leads to localized disruption of the flow by the particle diffusion and consequent maldistribution of fluid due to the combined effects of fluid and particle forces. As heat flux increases, the viscosity of the fluid decreases, and simultaneously, the thermal migration of the nanoparticles increases. The net effect leads to higher degrees of maldistribution. At high Re , inertia dominates within the flow regime and resistance to the random motion of particle is high. Thus, presence of particles in the base fluid does not affect the distribution of fluid among the channels to an appreciable extent. However, it is observed that the FMF tends to a plateau value as the concentration increases. At concentrations beyond 5 vol% (already in the high concentration regime), the effect of particle migration is greatly reduced by overcrowding and the viscosity of the overall fluid enhances drastically, leading to attainment of a saturation value for FMF. Several associated phenomena have been discussed in the subsequent sections where concentration maldistribution at enhanced temperatures has been dealt with in depth.

3.2.2 Concentration maldistribution

The extent of concentration maldistribution of the nanofluid as a function of Re and inlet concentration for both adiabatic and diabatic cases has been illustrated in Fig. 10. It can be inferred that although the trends of CMF variation for adiabatic and diabatic cases remain fairly similar,

Fig. 10 CMF (concentration maldistribution factor) variation for nanofluid at different inlet concentrations and Re for adiabatic flow and diabatic flows with 1 and 2 kW/m² applied heat fluxes (legend: *heat flux_concentration*)



they differ quantitatively. Also, several different phenomena in the distribution of particles crop up at elevated temperatures. At low Re , the CMF decreases at moderate heat flux and increases marginally at high heat fluxes, with the 5 % nanofluid being the exception wherein the CMF further falls at high heat flux. In low inertia flows, with the increase in fluid temperature, the decrease in fluid viscosity aids uniform distribution of particles. Due to lower viscosity, the particles experience reduced drag and therefore can diffuse more freely to achieve a more uniform particle distribution, despite flow maldistribution. However, further increase in heat flux leads to further lowering of viscous drag; the Brownian and thermophoretic diffusion/migration phenomena are enhanced, and thereby, the concentration maldistribution is more severely influenced by the non-isothermal temperature distribution within the fluid.

Another way of looking at the observed trends is from the particle migration point of view. In adiabatic case, the random motion of the particles is solely due to Brownian diffusion, whereas in diabatic case, it is due to both Brownian and thermophoretic migrations. Due to thermophoresis, the nanoparticles are directed away from the heated channel walls and the phenomenon is more predominant at the end channels because of the higher temperatures prevailing there due to flow maldistribution. Thermophoresis may oppose the random Brownian diffusion, providing the particles a net directional drift that overshadows the Brownian effect. Hence, added resistance to the random motion of particles leads to relatively more uniform distribution of concentration among the channels. At very high Re , the inertia of the flow enhances drastically with decreasing viscous forces and the flushing effect on the particles toward end channels essentially increases. However, in the case of moderate Re , the CMF shoots up even for moderate heat fluxes and then reduces when the flux increases. This is in all probability caused due to the sudden shift of particle

migration regimes from Brownian motion-controlled situation to Thermophoresis-controlled regime. At low Re , even drastic changes in viscosity cannot be expected to transit the flow regime from predominantly viscous to high inertia. Similarly, high Re flows remain predominantly inertia dominated. At moderate Re , where the flows are not dominated totally by either viscous or inertial regimes, a slight alteration in viscosity value can shift the flow to fully inertial regime or vice versa, leading to drastic localized particle maldistribution. This is possibly why the CMF increases suddenly even at moderate heat fluxes. However, at high heat flux, the viscous forces further decrease, thereby reducing the maldistribution as in high Re scenarios. Also, at high Re , Brownian fluctuations are effectively arrested by inertia and thermophoretic drift also reduces due to more uniform cooling at high flow velocities, resulting in similar concentration distribution among the channels for different inlet concentrations.

A more thorough picture of the effect of temperature on the distribution of the particulate phase can be envisioned by illustrating the effective concentration of the nanofluid entering each channel under different conditions. Figure 11 illustrates the effective concentration entering each microchannel at different heat flux level for a base flow equivalent to $Re = 5$ and an effective concentration of 5 vol% at the inlet manifold. It is observed from Fig. 11 that the effective concentration in the individual microchannels is different for different heat fluxes, thereby leading to variations in the CMF. Changes in the temperature field due to heat addition cause a shift in the concentration distribution pattern. It was seen earlier for the adiabatic condition the initial channels and the very last channel receive flows of appreciable concentration; under 1 kW/m² heating condition, a much better distribution is required among the central channels as well. As heat flux is applied, thermophoresis comes into the picture along with Brownian diffusion,

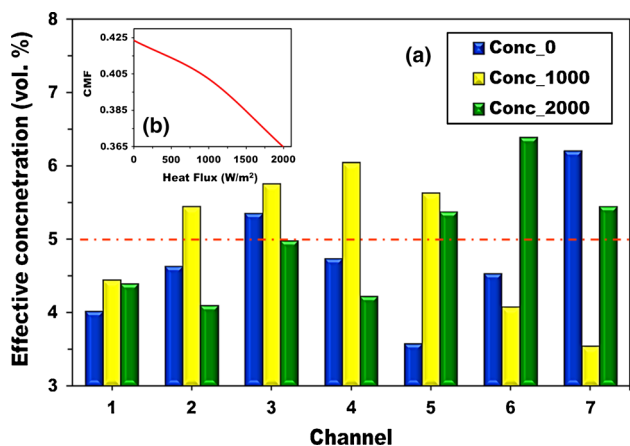


Fig. 11 **a** Effective concentration in individual microchannel for different heat fluxes for $Re = 5$ and concentrated nanofluid (5 vol%). **b** The behavior of the CMF (concentration maldistribution factor) at different heat fluxes for conditions equivalent to (a)

and since the Re is low, the resistance to the migration of the particles due to both the effects is less. Thermophoresis directs the particle population away from the manifold outer walls (due to less cooling than the channel side) and essentially toward the channels, causing the particles to distribute more uniformly among the channels than for adiabatic conditions. This is in agreement with the observations from Fig. 11. For increased heat flux, i.e., 2 kW/m^2 , the location of the valleys (low effective concentration) and peaks are qualitatively similar to the adiabatic case, except for the end channels. With increment in temperature, the effect of Brownian motion increases drastically and the directionality of the thermophoretic drift is overshadowed (but not obliterated) to some extent, leading to deteriorated distribution similar to those of adiabatic conditions. However, toward the end of the manifold, where the temperature gradients are higher due to flow maldistribution caused by

reduced viscosity, the thermophoretic drift regains upper hand and leads to better distribution than the adiabatic case.

The effect of temperature on the distribution of the particulate phase can also be qualitatively understood from the concentration contours within each channel. Figure 12 illustrates the same at a section located at the lengthwise central portion of the channels for different heat fluxes and for a nanofluid of 5 vol% with manifold flow corresponding to $Re = 5$. From the contours, it can be observed that at 0, 1 and 2 kW/m^2 the maximum effective concentration exists in channel 7, channel 4 and channel 6, respectively, and the minimum effective concentration can be observed in channel 5, channel 7 and channel 2, respectively (which are in agreement with the quantified data in Fig. 10a). It can further be seen that in the diabatic cases, especially for the later channels, there exist distinguishable regions of very low concentration near the side and bottom walls (such as in channels 5, 6 and 7 of 1 kW/m^2 and channels 6 and 7 of 2 kW/m^2). Such migration away from the heated channel walls is a clear evidence of thermophoretic drift, and it is strong in the later channels as these experience large thermal gradients caused by maldistribution in the base flow. The concentration within the front channels is more diffused due to the greater degree of mixing by the base flow. As the flow moves toward the later channels, it loses inertia and the particulate phase sluggishly drifts along, forming occasional clustered regions due to lack of inertia-induced mixing. However, as the viscous resistance reduces with temperature, the diffused contour can be seen to extend up to channel 4 in 2 kW/m^2 case as compared to channel 2 in the adiabatic case. Such observations provide firm support on the efficacy of nanofluids as future generation microdevice coolants.

Having discussed the distribution patterns of the nanoparticles in the individual channels and also the effect of temperature on the same, more insight can be shed on the

Fig. 12 Particle mass concentration distribution contours in individual channels at different heat fluxes for $Re = 5$ and 5 vol%

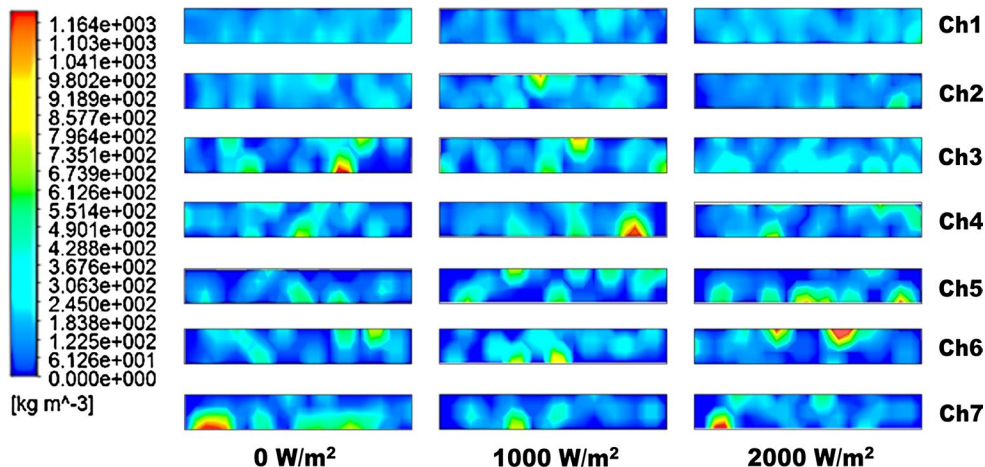
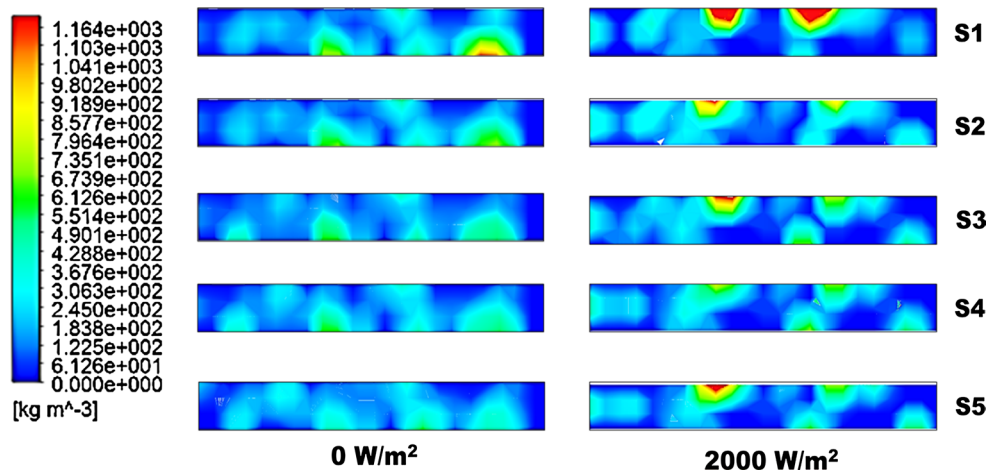


Fig. 13 Particle mass concentration contours of nanoparticles at $Re = 5$ and 5 vol% nanofluid in channel 3 and channel 5 at different cross sections for 0 and 2 kW/m², respectively. The channels have been so chosen since they have the same equivalent concentrations entering from the manifold (Fig. 11a)



subject matter by considering the effect of temperature on the cross-sectional distribution of the nanoparticles along a particular channel. Figure 13 illustrates the concentration variation over a cross section for the nanoparticles within channel 3 (for adiabatic conditions) and channel 5 (at 2 kW/m²). These cases have been meticulously chosen as these channels receive nanofluid flow of the same effective concentration (evident from Fig. 11). As observable, the distribution patterns in case of the adiabatic flow remain qualitatively similar, whereas that of the diabatic cases clearly show signs of redistribution and mixing. The fact that the particles tend to stay away from the heated bottom wall of the channel in the diabatic case further proves the vital effect of thermophoresis in particle distribution and subsequent heat transport. As the flow traverses toward the end of the channel, it gathers more heat and the Brownian flux increases, leading to more diffused distribution than that of the channel entrance regions.

3.2.3 Thermal performance

The cooling capability of the nanofluids is of course a major focus of the present article. Figure 14a, b illustrates the differences between the temperatures at the inlet and outlet in individual channels at a heat flux of 1000 W/m². The temperature drop at different Re for 5 vol% nanofluid has been shown in Fig. 14a. From the figure, it can be inferred that the temperature drop for initial channels is less when compared to those of end channels and this is because of non-uniform distribution of fluid due to flow maldistribution. Increase in Re enhances the heat transfer coefficient, and the increased inertia leads to better fluid distribution and less temperature drop across the channels. As discussed earlier, the presence of nanoparticles in base fluid leads to change in flow distribution among channels and this effect is more obvious at low Re and high concentrations (as illustrated in Fig. 3) and the same can also be

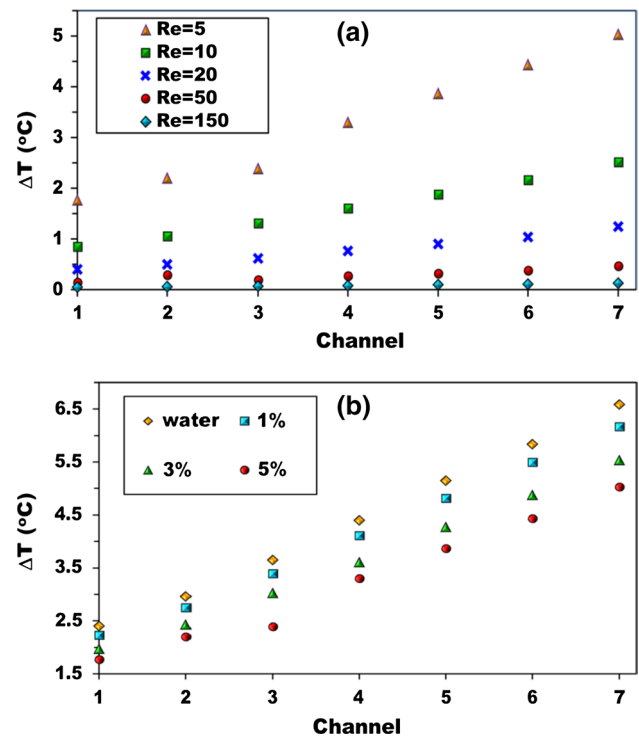


Fig. 14 Temperature difference between the inlet and the outlet of the channels at 1 kW/m², **a** temperature difference at different Re for 5 vol% nanofluid, **b** temperature difference at $Re = 5$ for water and different concentrations of nanofluid

observed in Fig. 14a, b. At high Re , the temperature drop in channels follows a linear variation, whereas the slope of the line gradually increases at low Re . For low inertia flow regimes ($Re = 5$), the temperature drop is higher toward the end channels which is caused by the higher degree of maldistribution of fluid and higher concentrations. The temperature drop in channels at different concentrations for $Re = 5$ has been shown in Fig. 14b, and it clearly demonstrates the effectiveness of nanofluids over conventional fluids.

As with the case of flow, the efficacy of the EPM and DPM in predicting heat transfer by nanofluids in microchannel systems also requires further probing. For this purpose, maximum temperatures occurring within the flow domain are considered and are illustrated in Fig. 15a. It can be observed that the results obtained from EPM analysis are consistently higher than those obtained from DPM analysis, and this difference increases with increase in heat load. Essentially, the figure further sheds light on the effectiveness of DPM in modeling convective transport in nanofluids. Since the maximum temperature within the domain is lower in case of DPM than EPM, it essentially means that the non-homogeneous nature of the nanofluids leads to efficient cooling of hotspots within the domain, thus establishing the ‘smart fluid’ characteristics of nanofluids and the efficacy of DPM in capturing the same. The EPM predicts higher degrees of thermal maldistribution compared to DPM, up to 5 °C in case of 5 kW/m² heat load and $Re = 5$, since it does not account for the particle migration effects. Effects such as enhanced Brownian and thermophoretic particle flux due to high heat flux lead to enhanced transport of heat from the channel walls to the bulk fluid. The particle distribution patterns are also modified (as discussed earlier), leading to more cooling, both in magnitude and in uniformity. It is only beyond Re values of 50 that the predictions by EPM are similar to those of DPM since in high velocity flows, the migration effects are arrested and the cooling essentially occurs due to increased mass flux of fluid. However, for microscale devices where low Re flows are expected in reality, such analysis is required for accurately predicting cooling capabilities of nanofluids as working fluids. A larger magnitude of the standard deviation of temperatures in a statistical population of data points in the domain essentially signifies more non-uniformity in the cooling characteristics. The differences between the standard deviations obtained for EPM and DPM-based computations have been illustrated in Fig. 15b. As observable from Fig. 15b, nanofluids are more effective cooling fluids than water, irrespective of the model employed for prediction. The caliber of the EPM can be seen to deteriorate with increasing concentration, and this is further evident that the particle migration and diffusive events are major governing parameters toward understanding thermofluidic performance of nanofluids.

Finally, having established the physics of flow distribution of nanofluids in parallel microchannel systems and the overall cooling effectiveness, it is imperative to mathematically predict the cooling capability of a given nanofluid for a particular geometry so as to reduce experimental trials for system optimization. The performance of a fluid in cooling a complex geometry can be assessed from the average temperature of the system and the standard deviation of a statistical population of temperatures. It has

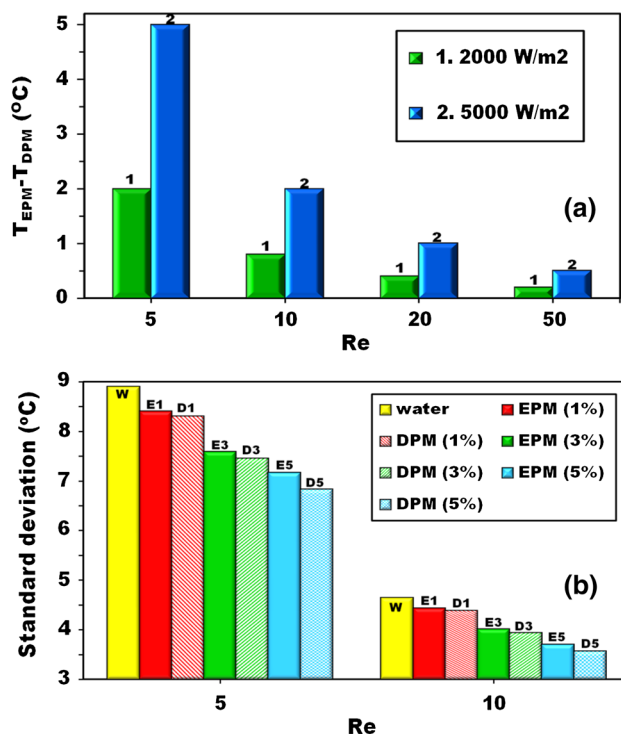


Fig. 15 Quantitative illustration of the efficiency of the DPM (discrete phase modeling) over the conventional EPM (effective property model) in prediction of thermofluidic features of nanofluid flows over a wide range of operating parameters. **a** Difference between the maximum temperatures, **b** standard deviation of the temperature

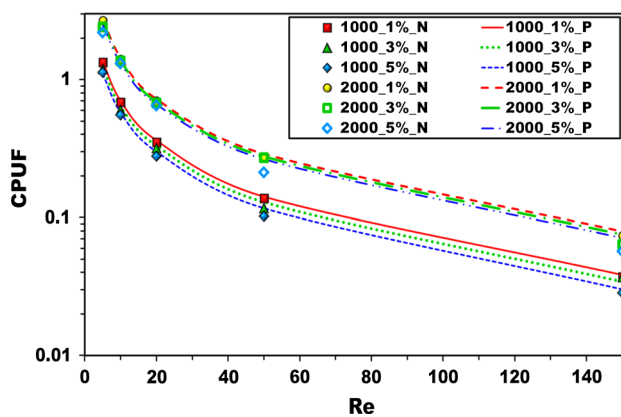


Fig. 16 Cooling performance prediction for nanofluids in microchannel heat exchanger systems

already been established that nanofluids are better coolants when the average temperature is concerned, as it is lower than that due to the base fluid itself. Furthermore, as shown in Fig. 15b, the standard deviation of the temperatures of a large number of points in the heated domain is also low in case of nanofluids, thereby proving that these fluids not only cool a system better but do the same in a much more

uniform fashion than normal fluids. However, the extent of this uniformity needs to be mathematically predicted in order to understand the effects of nanofluid concentration and flow domains on the cooling caliber. From the analysis of data, the standard deviation of the temperature drop in the channels (proposed here as the cooling performance uniformity factor) can be related to standard deviation for water as base fluid (at same Re); the Re and concentration are expressed as

$$\text{CPUF} = \sigma(\Delta T_{\text{ch,nf}})|_{Re} = \left\{ \sigma(\Delta T_{\text{ch,bf}})|_{Re} - \left(\frac{Re_{\text{crit}}}{Re} \right) \phi \right\} \quad (24)$$

The predictions obtained from the equation described above have been compared with respect to the predictions obtained from full-scale simulations, and the same have been illustrated in Fig. 16.

The uniformity parameter has been found to be a direct function of concentration, i.e., the reduction in standard deviation compared to that of water is higher when concentrated nanofluids are employed. While this sounds promising, very high concentrations lead to excessive pumping power and stability issues for the nanofluid particle agglomeration in reality. Accordingly, the concentration required to be optimal so as to obtain minimal increment in pumping power and maximum possible uniformity in cooling. Similarly, the inverse relation to the Re implies that flows of higher velocity lead to reduction in uniformity and this has been observed before, i.e., as Re increases, the behavior tends toward that of a homogeneous fluid. Accordingly, the Re also requires to be selected smartly so as to obtain maximal uniformity in cooling but should not be too low such that the average cooling performance deteriorates at the expense of uniformity. The effect of geometry comes into the picture through the critical Re value, which is purely dependent on the geometry. At low Re , the CMF increases with increment in concentration, and at higher Re , it decreases. The transit Re value at which the CMF becomes independent of the concentration is termed as the critical Re and can be deduced from analysis of simulation results. For the present geometry, this is determined to be ~ 30 and a clear scrutiny of Fig. 5 shows that the CMF is fairly constant for $Re = 50$, thus providing credibility to the obtained value.

4 Conclusions

The present article deals with the flow and concentration maldistribution of nanofluids in parallel microchannel systems. Reports in literature treat nanofluids as homogeneous single-phase fluids with enhanced effective properties and conclude improved cooling performance in such devices. However, experiments reveal that such predictions fall

short of the real fluid distribution and cooling performance. In particular, particle migration effects caused by Brownian motion, Thermophoresis and gradients of pressure or shear stress result in non-trivial variations in particle concentrations, particularly at low Re , dilute concentrations and for situations with heat transfer. Hence, a non-homogeneous two-phase model has to be utilized to model and understand nanofluid flow and associated heat transfer. In this article, an Eulerian–Lagrangian model for nanofluid flow in U configuration parallel microchannels has been considered and distribution of particles as well as the fluid and their impact vis-à-vis thermal performance has been reported. It has been observed that effective property model cannot be used to predict nanofluid performance in complex flow geometries as the distribution of particles and the fluid are interdependent on the distribution pattern of one another. This leads to grossly different flow distribution patterns and the effective particle concentration in the individual channels. The flow distribution has been observed to be more uniform at high heat fluxes. Essentially, this leads to ‘smart’ effects in terms of more uniform cooling in critical zones, and this is only predicted by the DPM formulation. The smart fluid effect refers to the compensation for the lack of coolant flow in certain zones of the channel assembly, by the appropriate modifications in nanoparticle concentrations as well as thermal conductivity (Li and Ahmadi 1992) to achieve uniform cooling. A mathematical predictive model has also been proposed to determine a quantitative measure of the uniformity of cooling performance of the nanofluid with water as base fluid. The proposed model well matches with numerical results at low heat flux conditions, whereas the simulations take care of temperature-dependent viscosity, but the model has no such provision, and hence, slight deviations are observed at high heat flux. The present findings can be utilized to obtain a priori estimates of nanofluid behavior within a particular microgeometry for optimizing flow and thermal performance in parallel microchannel heat sinks employing nanofluid coolants.

Acknowledgments The authors thank the Defense Research and Development Organization (DRDO) of India for partial financial support for the computational facilities. [Grant No. ERIP/ER/RIC/2013/M/01/2194/D (R&D)]. LSM would like to thank the Ministry of Human Resource Development (Govt. of India) for the doctoral scholarship. PD would like to thank IIT Madras for the postdoctoral fellowship (during previous affiliation).

References

- Anoop KB, Kabelac S, Sundararajan T, Das SK (2009) Rheological and flow characteristics of nanofluids: influence of electroviscous effects and particle agglomeration. *J Appl Phys* 106:034909
- Bassiouany MK, Martin H (1983a) Flow distribution and pressure drop in plate heat exchanger—I U-type. *Chem Eng Sci* 39(4):693–700

- Bassiouany MK, Martin H (1983b) Flow distribution and pressure drop in plate heat exchanger—II Z-type. *Chem Eng Sci* 39(4):701–704
- Bejan A, Morega AM (1993) Optical arrays of pin fins and plate fins in laminar forced convection. *ASME J Heat Transf* 115(1):75–81
- Chen C-H, Ding C-Y (2011) Study on the thermal behavior and cooling performance of a nanofluid-cooled microchannel heat sink. *Int J Therm Sci* 50:378–384
- Choi SUS, Eastman JA (1995) Enhancing thermal conductivity of fluids with nanoparticles. In: Proceedings of the 1995 ASME international mechanical engineering congress and exposition, San Francisco
- Das SK, Putra N, Thiesen P, Roetzel W (2003) Temperature dependence of thermal conductivity enhancement for nanofluids. *ASME J Heat Transf* 125(4):567–574
- Das SK, Choi SUS, Patel HE (2006) Heat transfer in nanofluids—a review. *Heat Transf Eng* 27(10):3–19
- Dhar P, Ansari H, Sengupta S, Siva VM, Pradeep T, Pattamatta A, Das SK (2013a) Percolation network dynamicity and sheet dynamics governed viscous behavior of poly dispersed graphene nanosheet suspensions. *J Nanopart Res* 15(12):1–12
- Dhar P, Sengupta S, Chakraborty S, Pattamatta A, Das SK (2013b) The role of percolation and sheet dynamics during heat conduction in poly dispersed graphene nanofluids. *Appl Phys Lett* 102(16):163114
- FLUENT 12.0 User manual (2016) ANSYS FLUENT
- Hung TC, Yan W-M, Wang X-D, Chang C-Y (2012) Heat transfer enhancement in microchannel heat sinks using nanofluids. *Int J Heat Mass Transf* 55:2559–2570
- Jones BJ, Lee P, Garimella SV (2008) Infrared micro-particle image velocimetry measurements and predictions of flow distribution in a microchannel heat sink. *Int J Heat Mass Transf* 51(7–8):1877–1887
- Judy J, Maynes D, Web BW (2002) Characterization of frictional pressure drop for liquid flows through microchannels. *Int J Heat Mass Transf* 45(17):3477–3489
- Kalteh M, Abbassi A, Saffar-Avval M, Harting J (2011) J Eulerian–Eulerian two-phase numerical simulation of nanofluid laminar forced convection in a microchannel. *Int J Heat Fluid Flow* 32:107–116
- Koo J, Kleinstreuer C (2004) A new thermal conductivity model for nanofluids. *J Nanopart Res* 6:577–588
- Kumaraguruparan G, Kumaran RM, Sornakumar T, Sundarajan T (2011) A numerical and experimental investigation of flow maldistribution in a microchannel heat sink. *Int Commun Heat Mass Transf* 38(10):1349–1353
- Lee S, Choi SUS, Li S, Eastman JA (1999) Measuring thermal conductivity of fluids containing oxide nanoparticles. *ASME J Heat Transf* 121:280–289
- Li A, Ahmadi G (1992) Dispersion and deposition of spherical particles from point sources in a turbulent channel flow. *Aerosol Sci Technol* 16(4):209–226
- Maharudrayya S, Jayanti S, Deshpande AP (2006) Pressure drop and flow distribution in multiple parallel channel configuration used in PEM fuel cell stacks. *J Power Sour* 157(1):358–367
- Mohammed HA, Bhaskaran G, Shuaib NH, Saidur R (2011) Heat transfer and fluid flow characteristics in microchannel heat exchangers using nanofluids—a review. *Renew Sust Energy Rev* 15(3):1502–1512
- Ounis H, Ahmadi G, McLaughlin JB (1991) Brownian diffusion of submicrometer particles in the viscous sublayer. *J Colloid Interface Sci* 143(1):266–277
- Özeringç S, Kakaç S, Yazıcıoğlu AG (2010) Enhanced thermal conductivity of nanofluids: a state-of-the-art review. *Microfluid Nanofluid* 8:145–170
- Qu W, Mala GM, Li D (2000) Pressure driven water flows in trapezoidal silicon microchannels. *Int J Heat Mass Transf* 43(3):353–364
- Raisi A, Ghasemi B, Aminossadati SM (2011) A numerical study on the forced convection of laminar nanofluid in a microchannel with both slip and no-slip conditions. *Num Heat Transf A Appl* 59:114–129
- Saffman PG (1965) The lift on a small sphere in a slow shear flow. *J Fluid Mech* 22:385–400
- Salman BH, Mohammed HA, Munisamy KM, Kherbeet ASH (2013) Characteristics of heat transfer and fluid flow in microtube and microchannels using conventional fluids and nanofluids: a review. *Renew Sust Energy Rev* 28:848–880
- Seghal SS, Murugesan K, Mohapatra SK (2011) Experimental investigation of the effect of flow arrangements on the performance of a micro-channel heat sink. *Exp Heat Transf* 24(3):215–233
- Singh PK, Harikrishna PV, Sundarajan T, Das SK (2011) Experimental and numerical investigation into the heat transfer study of nanofluids in microchannel. *ASME J Heat Transf* 133(12):121701-1–121701-9
- Siva MV, Pattamatta A, Das SK (2013) A numerical study of flow and temperature maldistribution in a parallel microchannel system for heat removal in microelectronic devices. *ASME J Therm Sci Eng Appl* 5(4):041008-1–041008-8
- Siva MV, Pattamatta A, Das SK (2014) Investigation on flow maldistribution in parallel microchannel systems for integrated microelectronic device cooling. *IEEE Trans Compon Packag Manuf Technol* 4(3):438–450
- Talbot L, Cheng RK, Schefer RW, Willis DR (1980) Thermophoresis of particles in a heated boundary layer. *J Fluid Mech* 101(4):737–758
- Tuckerman DB, Pease RFW (1981) High performance heat sinking for VLSI. *IEEE Electron Device* 2(5):126–129
- Weilin Q, Mudawar I (2002) Analysis of three-dimensional heat transfer in micro-channel heat sinks. *Int J Heat Mass Transf* 45(19):3973–3985